ACS APPLIED MATERIALS & INTERFACES

Research Article

www.acsami.org

Micelles of *d*-α-Tocopheryl Polyethylene Glycol 2000 Succinate (TPGS 2K) for Doxorubicin Delivery with Reversal of Multidrug Resistance

Tangna Hao,[‡] Dawei Chen,[§,∥] Kexin Liu,[†] Yan Qi,[†] Yan Tian,[†] Pengyuan Sun,[†] Yuanhong Liu,[†] and Zhen Li*[,†]

[†]School of Pharmacy, Dalian Medical University, Dalian 116044, PR China

[‡]Department of Pharmacy, The Second Affiliated Hospital of Dalian Medical University, Dalian 116011, PR China

[§]Department of Pharmaceutics, School of Pharmacy, Shenyang Pharmaceutical University, Shenyang 110016, PR China

[∥]School of Pharmacy, Medical College of Soochow University, Suzhou 215123, PR China

Supporting Information

ABSTRACT: The purpose of this study is to investigate the ability of doxorubicin (DOX)-loaded *d*-α-tocopheryl polyethylene glycol 2000 succinate (TPGS 2K) micelles to overcome MDR in breast cancer treatment. The DOX-loaded TPGS 2K micelles exhibited an average size of around 23 nm, a near neutral zeta potential of around 4 mv and high encapsulation efficiency (85.22 ± 1.89%). The TPGS 2K conjugate did not have significant influences on the reduction of mitochondrial membrane potential (MMP) and the depletion of intracellular ATP level of MCF-7/ADR cells but had an evident effect on the inhibition of Verapamil-induced P-gp ATPase activity. In vitro cell culture experiments demonstrated the DOX-loaded TPGS 2K micelles, resulting in higher cellular uptake and more significant cytotoxicity effect against MCF-7/MDR cells than the free DOX solution. Additionally, the in vivo imaging study revealed DiR-loaded TPGS 2K micelles distributed selectively in MCF-7/ADR tumor-bearing nude mice and had a sufficient residence time. In the anticancer efficacy test with MCF-7/ADR tumor bearing nude mice, the DOX-loaded TPGS 2K micelles displayed significantly higher antitumor activity compared with free DOX solution at the same DOX dosage but less toxicity evaluated by the change of body weight and histological examination. Therefore, this drug delivery micellar system based on TPGS 2K conjugates can serve as a potential nanomedicine for reversing MDR.

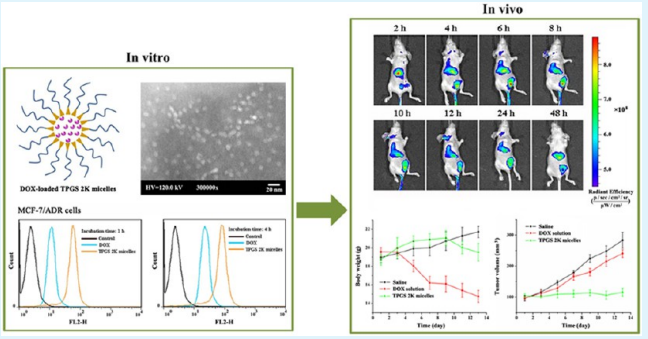

KEYWORDS: *self-assembled micelles, doxorubicin, TPGS 2K, multidrug resistance, drug delivery, chemotherapy*

1. INTRODUCTION

The emergence of multidrug resistance (MDR) is a major obstacle in cancer chemotherapy. In past years, various mechanisms of MDR have been reported, including increased drug efflux due to a superfamily of ATP binding cassette (ABC) proteins, metabolic modification and detoxification, activation of DNA repair, alteration in drug-induced apoptosis owing to the change of the Bcl-2 pathway, the sequestration of drugs within cytoplasmic vesicles, and existence of cancer stem cells.[1−3] Among these mechanisms, the overexpression of drug efflux pumps, especially for P-glycoprotein (P-gp), is one of the major causes of MDR and most extensively studied.[4,5] A number of ABC transporter inhibitors have been used to resensitize MDR cells in preclinical and clinical studies. Unfortunately, the results of these on clinical trials were not so satisfactory due to limited therapeutic performance, unacceptable systemic toxicity, and so on.[6,7]

Polymeric micelles systems have attracted great interest in recent years for surmounting the MDR of tumors by circumventing P-gp-mediated efflux. Amphiphilic polymers can self-assemble in aqueous solution to generate shell−core nanostructured micelles. Such shell−core structures could improve solubility of poor water-soluble drugs and stabilize the drugs within the hydrophilic corona. The micellar drug formulations have the ability to prolong drug circulation time, improve cell- or tissue-specific targeting, and decrease systemic side effects.[8−12] A number of natural and synthetic biomaterials have been used to prepare nanocarriers to enhance cellular accumulation of anticancer drugs to reverse MDR. Unfortunately, some intracellular drug molecules could still be pumped out by efflux proteins because the common polymeric nanomaterials themselves have no obvious effect on inhibiting the efflux pump.[13,14] Therefore, the selected polymer nanomaterials could serve as inert carriers as well as biological response modifiers (such as effects on cell respiration and ATPase activity of drug efflux transporters).[15] Some nonionic

Received: June 6, 2015
Accepted: July 27, 2015
Published: July 27, 2015

DOI: 10.1021/acsami.5b04995
ACS Appl. Mater. Interfaces 2015, 7, 18064−18075

surfactants (such as *d*-α-tocopheryl polyethylene glycol 1000 succinate (TPGS) and Pluronic block copolymers) showed the ability to reverse MDR.[16−18] A series of nanoformulations based on nonionic surfactants have been designed to deliver anticancer drugs and sensitize MDR cells.

TPGS is an excellent surfactant used in pharmaceutical formulations as an absorption enhancer, emulsifier, drug solubilizer, stabilizer, and as a component material for construction of the nanocarriers.[19] Modification of polymeric nanoparticles with TPGS can improve drug encapsulation efficiency, promote cellular uptake of anticancer drugs, extend blood circulation time, and enhance the bioavailability of anticancer drugs.[20−22] Furthermore, TPGS could serve as an inhibitor of *P*-glycoprotein for oral drug delivery as well as for overcoming MDR.[23−25] TPGS can also be utilized to form micelles for application in anticancer drug delivery. Muthu M. S. et al. constructed docetaxel-loaded TPGS micelles for glioma chemotherapy. For this purpose, they made use of PEG because of its long circulation half-life and vitamin E because of its efficient uptake by cells.[26] The results demonstrated that docetaxel-loaded TPGS micelles at different loading levels had lower IC50 values compared to Taxotere after incubation for 24 h with C6 glioma cells. Although TPGS possesses micellar properties, some characters limit its further application as drug carrier. The relatively high CMC value (0.2 mg/mL) of TPGS suggests that the TPGS micelles could dissociate readily in plasma.[27] Meanwhile, the PEG 1000 chain of TPGS is not sufficiently long to ensure prolonged circulation of micelles in vivo.[28] In this work, the *d*-α-tocopheryl polyethylene glycol 2000 succinate (TPGS 2K) was synthesized through reaction between *d*-α-tocopheryl succinate and methoxy poly(ethylene glycol) 2000-amine (MPEG2000-NH_2). The lipophilic structure of vitamin esuccinate is retained in the structure of TPGS 2K. The hydrophilic head of PEG 2000 ensures the formed micelles to minimize nonspecific phagocytic uptake and thus extend blood circulation time. The TPGS 2K micelles were prepared for anticancer drug delivery with doxorubicin (DOX) as a model drug. A systematic evaluation of the antitumor efficacy, and reversing MDR mechanisms of the DOX-loaded TPGS 2K micelles was performed at the cellular and animal levels. Such micelles were proved to formulate DOX effectively, overcome MDR, and induce an improved anticancer efficacy as expected.

2. MATERIALS AND METHODS

2.1. Materials. DOX·HCl was supplied by HuaFeng United Technology Co. Ltd. (Beijing, China). Methoxypolyethylene glycol amine 2000 was purchased from Seebio Biochemical, Inc. (Shanghai, China). Pyrene and Hoechst 33342 were obtained from Sigma (St. Louis, MO). Vitamin E succinate was purchased from Yuancheng Gongchuang Technology Co. Ltd. (Wuhan, China). 1-(3-(Dimethylamino)propyl)-3- ethylcarbodiimide hydrochloride (EDC·HCl) and *N*-hydroxysuccinimide (NHS) were obtained from GL Biochem. Co. Ltd. (Shanghai, China). MCF-7 and MCF-7/ADR cells were supplied by American Type Culture Collection (ATCC, Rockville, MD). Tetrahydrofuran (THF), dichloromethane (DCM), methanol, and acetone were obtained from Bodi Drug Manufacturing Co. Ltd. (Tianjin, China).

2.2. Synthesis of TPGS 2K. VES, NHS, and EDC·HCl were dissolved in 10 mL anhydrous DCM with the molar ratio of 1:1.2:1.2. The mixture was stirred at room temperature for 4 h to preactivate the carboxyl group of VES. Then, weighted amount of methoxypolyethylene glycol amine 2000 was added into the above solution under stirring at room temperature. The reaction was continued for 48 h under a nitrogen atmosphere. After reaction, the reacted product was precipitated in excess cold diethyl ether to remove the excess VES. The precipitate was dissolved in DMSO and then dialyzed against water for 72 h through a dialysis bag of MWCO 1000 Da. The final TPGS 2K conjugate was then obtained by lyophilization as a white powder.

2.3. Characterization of TPGS 2K. The compositions of TPGS and TPGS 2K were confirmed by ^{1}H NMR in $CDCl_3$ at 300 Hz (Bruker ARX-300, Germany). Meanwhile, FT-IR spectra (Bruker IFS-55 spectrometer, Switzerland) in the range of the 4000 to 400 cm^{-1} region were obtained for TPGS and TPGS 2K samples.

2.4. Measurement of the Critical Micellar Concentration (CMC). The CMC value of TPGS 2K conjugate was determined by the pyrene-based fluorescence probe technique. Briefly, 0.5 mL of 6.0 × 10^{-7} mol/L solution of pyrene in acetone was added individually to 10 mL volumetric flasks. The acetone was left to evaporate under a nitrogen stream to form a pyrene film in the volumetric flask. After that, a series of aqueous TPGS 2K solutions (1 × 10^{-4} mg/mL to 0.1 mg/mL) were mixed with pyrene on a shaker at 37 °C for 24 h to reach a final pyrene concentration of 3.0 × 10^{-8} mol/L. The fluorescence spectra were recorded using a fluorescence spectrophotometer (F-2500, Hitachi, Japan). The change of the intensity ratio (I_{338}/I_{334}) of pyrene versus log polymer TPGS 2K concentration was plotted from excitation spectra from 300 to 350 nm at an emission wavelength of 397 nm. The CMC value was calculated from the cross-point of two straight lines fitted through the points of the flat and remarkably increasing region, respectively.

2.5. Preparation of Drug-Loaded TPGS 2K Micelles. DOX-loaded TPGS 2K micelles were prepared by thin-film hydration method. First, DOX·HCl was stirred with 5 mol equiv of triethylamine in methanol overnight to form the DOX base. Then a total of 20 mg TPGS 2K and a given amount of DOX were dissolved in 10 mL THF. The solvent was evaporated by rotary evaporation at 60 °C for 1 h to obtain a thin film, which was hydrated in 2 mL of water at 60 °C for 30 min. The resultant micelle solution was filtered through a 0.22 μm filter to remove the nonencapsulated DOX aggregates. For DiR-loaded TPGS 2K micelles, they were prepared with a similar procedure.

2.6. Particle Size, Size Distribution, and Zeta Potential Analysis. The particle size, size distribution, and zeta potential of micelles were analyzed by a Nano-2S90 Zeta Sizer (Malvern Instruments, U.K.). The measurements were performed in triplicate.

2.7. Transmission Electron Microscopy (TEM). The sample was prepared by administering one drop of DOX-loaded TPGS 2K micellar solution onto a copper grid and then negatively stained with 2.0% (w/v) phosphotungstic acid. After air-drying for 30 min, the morphology of the sample was observed using a transmission electron microscope (Jeol JEM-2000EX, Tokyo, Japan).

2.8. Drug Loading Content and Entrapment Efficiency. To measure DOX loading content (DL%) and entrapment efficiency (EE %), the DOX-loaded micellar solution was destroyed by adding an appropriate volume of DMSO and then assayed by a UV−vis spectrophotometer at 481 nm. The unloaded DOX was separated using 10000 MWCO ultrafiltration membrane (Millipore, Billerica, MA) followed by determining the absorbance at 481 nm as described above. The DL% and EE% were calculated by the following equation, respectively.[29]

$$\mathrm{DL\%} = \frac{\text{weight of the drug in micelles}}{\text{total weight of the loaded drug and polymer}} \times 100\%$$

$$\mathrm{EE\%} = \frac{\text{weight of the drug in micelles}}{\text{weight of the feeding drug}} \times 100\%$$

2.9. In Vitro Drug Release. In vitro release profiles of DOX from TPGS 2K micelles were performed as follows: 2 mL of DOX micellar solution was transferred to a dialysis bag (MWCO 3500 Da), and dialyzed against 25 mL of PBS (pH 5.0 and 7.4) at 37 °C under horizontal shaking at 100 rpm. Periodically, 3 mL aliquots were withdrawn and replaced by 3 mL fresh PBS. The released DOX content was analyzed by UV−vis spectrometry at 481 nm. The results are presented as mean ± SD obtained from 3 samples.

DOI: 10.1021/acsami.5b04995
ACS Appl. Mater. Interfaces 2015, 7, 18064−18075

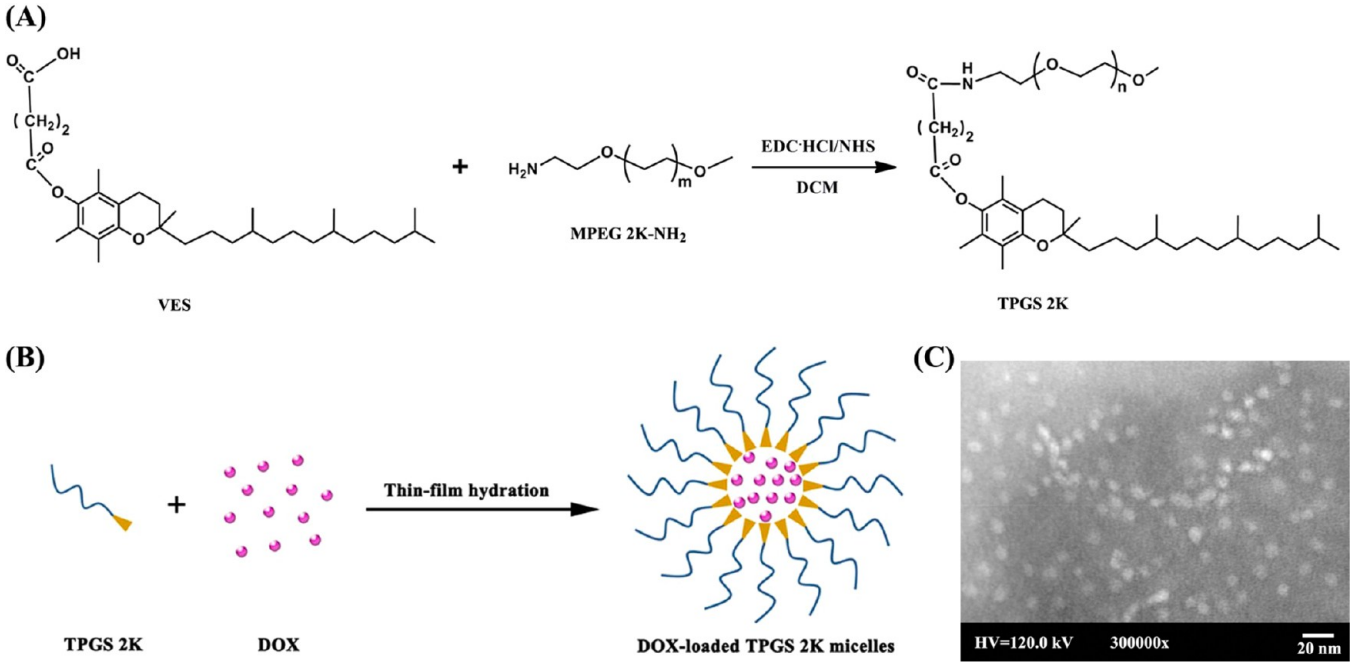

Figure 1. (A) The synthesis scheme of TPGS 2K conjugate. (B) Schematic illustration of DOX-loaded TPGS 2K micelles. (C) TEM image of the DOX-loaded TPGS 2K micelles.

2.10. Assay of P-gp ATPase Activity. The modulation of P-gp ATPase activity by TPGS 2K or TPGS was analyzed using the P-gp-Glo assay system (Promega). Briefly, test samples containing verapamil (50 μM) and polymer (TPGS or TPGS 2K, final concentrations at 10, 20, 50, and 100 μM, respectively) or Na_3VO_4 were added to 96-well plates and incubated with recombinant human P-gp membrane for 5 min at 37 °C. MgATP was then added into the above samples, followed by incubation at 37 °C for 40 min to initiate the reaction. Thereafter, the resultant samples were mixed with ATP detection reagent and then incubated for 20 min at room temperature to develop the luminescence. Finally, the luminescence was measured by a multifunctional microplate reader (Tecan, Austria). The changes of relative light unit (ΔRLU) were calculated by comparing the mixture of polymer and verapamil-treated samples with the Na_3VO_4-treated samples.

2.11. Assay of Mitochondrial Membrane Potential. Mitochondrial membrane potential was measured using a JC-1 Apoptosis Detection Kit (Beyotime, Nantong, China). MCF-7/ADR cells were seeded in 12-well plates (2×10^5 cells/well) and incubated overnight. Then the cells were incubated in fresh culture medium containing TPGS or TPGS 2K (50 μM) for 3 h. Subsequently, the cells were trypsinized, rinsed twice with cold PBS, and resuspended in a 500 μL JC-1 working solution for 20 min. All samples were then rinsed twice with 1× incubation buffer and immediately analyzed using a multifunctional microplate reader (Tecan, Austria) to detect green fluorescence at excitation/emission wavelengths of 490/530 nm and red fluorescence at excitation/emission wavelengths of 525/590 nm. The obtained values were expressed as an average JC-1 red/green signal intensity ratio (n = 3).

2.12. Intracellular ATP Level Assay. MCF-7/ADR cells were seeded in 12-well plates (2×10^5 cells/well) and grown for 24 h to allow cell attachment. Following treatment with 50 μM TPGS or TPGS 2K solution for 3 h, the cells were rinsed twice with PBS and solubilized in an ATP lysis buffer. The kit based on the luciferin/luciferase assay (Beyotime, Nantong, China) was used for determining the ATP level in cell lysate. The luminescence was measured by the multifunctional microplate reader (Tecan, Austria). ATP concentrations were calculated by an ATP standard calibration curve and normalized by protein content in each sample determined by a BCA kit (Beyotime, Nantong, China).

2.13. MTT Assay. MCF-7 or MCF-7/ADR cells were seeded in 96-well plates in 100 μL of medium to obtain a concentration of 10000 cells per well, followed by an incubation for 24 h. The cells were then treated with free DOX solution, DOX-loaded TPGS 2K micelles, or blank TPGS 2K micelles diluted with culture medium to various concentrations for 24, 48, and 72 h at 37 °C. Then cytotoxicity was assessed using the MTT method. The formed MTT-formazan crystals were dissolved in DMSO, followed by measuring the absorbance at 570 nm. The cell viability (%) was calculated based on optical density values of sample wells versus reference wells containing only cell culture media.

2.14. Cellular Uptake Studies. MCF-7 and MCF-7/ADR cells were seeded onto glass coverslips placed in 6-well culture plates (3×10^5 cells/well) and incubated for 24 h. DOX-loaded TPGS 2K micelles or DOX solution in 2 mL of PBS were added to each well (DOX concentration: 10 μg/mL). After incubation for 1 and 4 h, the cells were rinsed with cold PBS for three times and then stained with Hoechst 33342 for 10 min. The cells were further washed twice with cold PBS and fixed by 4% formaldehyde for 20 min. The coverslips were further washed twice with cold PBS. Fluorescence images of cells were observed using a confocal microscope (CLSM, Zeiss LSM 710, Carl Zeiss, Germany).

For quantitative analysis, the intensity of DOX fluorescence on cellular uptake was determined using a FACS Calibur flow cytometer (Becton Dickinson, San Jose, CA). The cells were harvested using trypsin-EDTA, then washed and resuspended in PBS. For each sample, a minimum of 10000 cells were collected and then analyzed using Cell Quest software.

2.15. In Vivo Imaging. MCF-7/ADR cells (1×10^7 cells cells/each mouse) were subcutaneously injected into the flanks of female BALB/c nude mice (18−20 g) for constructing the tumor-bearing mice. 0.2 mL of DiR-loaded TPGS 2K micelles was intravenously injected through a tail vein. The whole body fluorescence imaging of nude mice bearing the MCF-7/ADR tumor was carried out using an IVIS Lumina II Imaging System (Caliper Life Sciences, Hopkinton, MA) at the time points of 1, 2, 4, 8, 12, 24, and 48 h post injection with the excitation wavelength of 745 nm. After 48 h, the nude mice were sacrificed, and the major organs and tumors were isolated from the animals for ex vivo fluorescence imaging.

2.16. In Vivo Antitumor Effect. MCF-7/ADR cells were introduced to female BALB/c nude mice as described above. The

DOI: 10.1021/acsami.5b04995
ACS Appl. Mater. Interfaces 2015, 7, 18064−18075

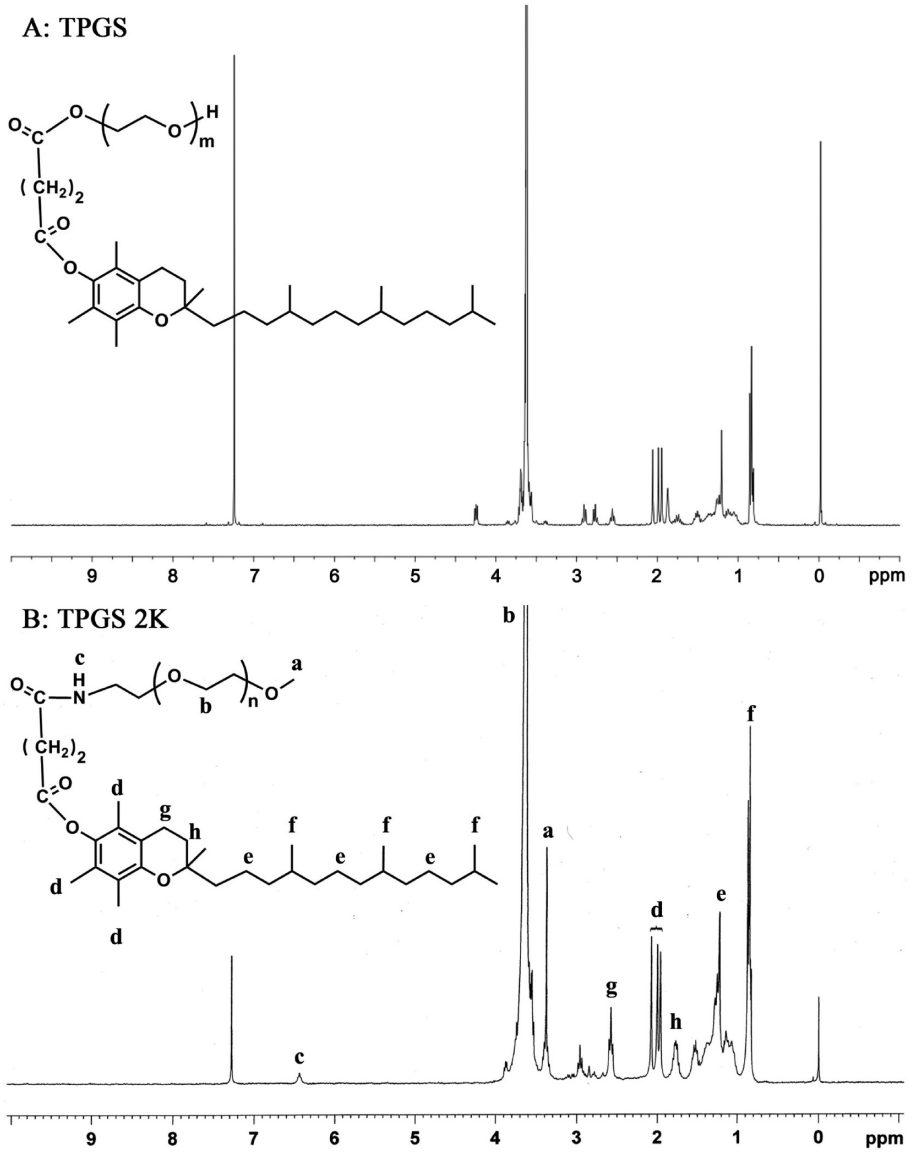

Figure 2. Typical ^{1}H NMR spectra of (A) TPGS and (B) TPGS 2K.

tumors were allowed to grow to around 100 mm^3 before the experiment. The mice were randomly assigned to three groups (n = 5) and injected intravenously once 3 days with saline, DOX solution, and DOX-loaded TPGS 2K micelles at a dose of 10 mg DOX/kg. Tumor volume and body weight were monitored every 2 days over a period of 13 days. At the end of the experiment, all treatment and control nude mice were executed and the tumors were harvested and weighed. The heart tissues were also collected, fixed in 4% formaldehyde for histological examination. The tumor inhibition rate (TIR) was calculated by the following formula:

$$\mathrm{TIR}(\%) = [(W_c - W_d)/W_c] \times 100\%$$

where W_c is the average tumor weight after the treatment with saline and W_d is that after treatment with the drug.

2.17. Statistical Analysis. Data were presented as mean ± SD. Statistical comparisons were determined by the analysis of variance (ANOVA) among ≥3 groups or Student's t test between 2 groups. P values less than 0.05 were considered to be statistically significant.

3. RESULTS AND DISCUSSIONS

3.1. Synthesis and Characterization. TPGS 2K conjugate was synthesized via an amidation reaction at room temperature (Figure 1A). The chemical structure of TPGS 2K were characterized by ^{1}H NMR in $CDCl_3$. The characteristic signals of TPGS 2K were similar to that of TPGS (Figure 2). Peak a at 3.38 ppm and peak b at 3.65 ppm were assigned to $-OC\underline{H}_3$ protons and $-OC\underline{H}_2C\underline{H}_2O-$ protons of the MPEG segment, respectively; peak c at 6.42 ppm was ascribed to the amide proton (−NH−CO−) from the amidation reaction; peak f at 0.86 ppm was for the $-C\underline{H}_3$ protons of the long-chain alkyl group of TPGS 2K. The peaks in the aliphatic region (signal at 2.58 ppm; signals at 2.08−1.96 ppm; signal at 1.78 ppm; signal at 1.26 ppm) were assigned to various moieties of the vitamin E tail of TPGS 2K.

The FT-IR spectra of TPGS and TPGS 2K conjugate are shown in Figure S1. The spectrum of TPGS showed characteristic peaks at 2888.2 (C−H stretching band), 1737.5 (ester C═O stretching band), and 1114.7 cm^{-1} (C−O−C stretching band). For the synthesized TPGS 2K conjugate, the ester C═O stretching band was decreased in intensity and shifted to 1751.8 cm^{-1}. The obvious amide C═O stretching band appeared at 1650.1 cm^{-1}, indicating the existence of amide linkage in the structure of TPGS 2K conjugate.

DOI: 10.1021/acsami.5b04995
ACS Appl. Mater. Interfaces 2015, 7, 18064−18075

Table 1. Characterization of Blank TPGS 2K Micelles and DOX-Loaded TPGS 2K Micelles

micelles	DL (%)	EE (%)	particle size (nm)	polydispersity	zeta potential (mv)
blank micelles	N/A	N/A	15.4 ± 2.2	0.124 ± 0.011	1.37 ± 0.20
DOX-loaded micelles	9.62 ± 0.19	85.22 ± 1.89	23.4 ± 1.7	0.309 ± 0.016	4.31 ± 0.73

3.2. CMC Determination. The synthesized TPGS 2K conjugates could be self-assembled in aqueous solution to form nanomicelles (Figure 1B). The CMC value of the TPGS 2K conjugate was obtained by fluorescent determination using pyrene as a probe. Figure S2 showed a typical plot of intensity ratio I_{338}/I_{334} versus lg(C) of TPGS 2K. The CMC value of TPGS 2K calculated from the plot was 1.78 μg/mL. The calculated CMC value was significantly lower than that of TPGS (0.2 mg/mL) as reported in ref 27. It suggests that the TPGS 2K micelles have better physical integrity and dilution stability after intravenously injected into the bloodstream for systemic circulation compared with TPGS micelles.

3.3. Preparation and Characterization of TPGS 2K Micelles. The drug encapsulation efficiency and drug loading content of DOX-loaded TPGS 2K micelles were measured to be 85.22% and 9.62%, respectively, indicating the good compatibility between DOX and the hydrophobic inner core of TPGS 2K micelles (Table 1). This result is satisfactory for constructing an efficient DOX delivery system. The transmission electron microscopy (TEM) image showed that the micelles were generally spherical in shape with good monodispersity (Figure 1C). The mean hydrodynamic diameter of blank and DOX-loaded TPGS 2K micelles measured by dynamic light scattering were 15.4 and 23.4 nm, respectively (Table 1). The DOX molecules trapped into the TPGS 2K micelles led to an increase in micellar size. The mean hydrodynamic size of drug-loaded TPGS 2K micelles is in the desired size range for accumulating in tumor vasculature through the EPR effect.[30−33] The zeta potentials were near neutral for both blank and DOX-loaded TPGS 2K micelles (1.37 ± 0.20 and 4.31 ± 0.73 mV) due to the shielding effect of the neutrally charged PEG shell.[34]

3.4. In Vitro Drug Release. In vitro drug release profiles from DOX-loaded TPGS 2K micelles were evaluated at a physiological pH (7.4) and a lysosomal pH (5.0) at 37 °C (Figure 3). The DOX-loaded TPGS 2K micelles displayed biphasic drug release profiles under different pH conditions with an initial fast release phase followed by a controlled release phase. Meanwhile, the DOX release from TPGS 2K micelles was pH-dependent. At 12 h, the cumulative drug release of TPGS 2K micelles at pH 5.0 (41.60 ± 1.90%) was higher than that at pH 7.4 (27.58 ± 1.89%) ($p < 0.01$). In the following 12 h, the cumulative release percent reached 47.20 ± 1.27% (at pH 5.0) and 28.28 ± 2.11% (at pH 7.4), respectively ($p < 0.01$). The DOX release from TPGS 2K micelles was slow at normal physiological pH (pH 7.4) and accelerated at lysosomal pH (5.0). This result may be ascribed to the protonation of DOX at acidic condition and the acid-catalyzed cleavage of the azomethine bond in DOX−DOX. Such a pH-dependent release characteristic may be beneficial to ensure the intracellular DOX release due to a decreased pH in the endolysosomes within tumor cells.[35]

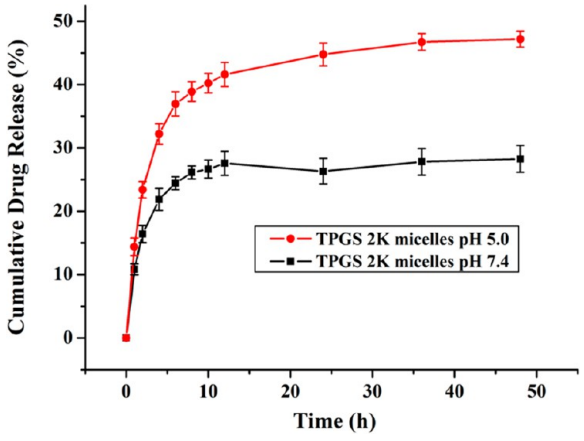

Figure 3. In vitro release profiles of DOX-loaded TPGS 2K micelles in PBS (pH 7.4 and 5.0) at 37 °C.

3.5. Inhibition of P-gp ATPase. The Pgp-Glo system (Promega) was used to detect the effects of compounds on recombinant human P-gp in a cell membrane fraction. Na_3VO_4 enclosed in the assay kit is a selective inhibitor of P-gp, and samples treated with Na_3VO_4 exhibit no P-gp ATPase activity. Additionally, verapamil enclosed in the assay kit is a P-gp substrate which stimulates P-gp ATPase activity (consuming ATP). Decrease in the consumption of ATP (ΔRLU) represents the decrease of activity of ATPase and the inhibition of P-gp.[36] The assay relies on the ATP dependence of the light-generating reaction of firefly luciferase. Both TPGS and TPGS 2K significantly inhibited the verapamil-stimulated P-gp ATPase activity in a concentration-dependent manner. Lower ΔRLU was achieved by higher copolymer concentration. Verapamil-stimulated ATPase activity with TPGS 2K inhibition is comparable to TPGS at every of the designed copolymer concentrations except the one at 100 μM (Figure 4). This result was basically in accordance with the published work.[37] The P-gp-mediated drug efflux is dependent on drug substrate interaction with P-gp and ATP hydrolysis by P-gp ATPase.[38]

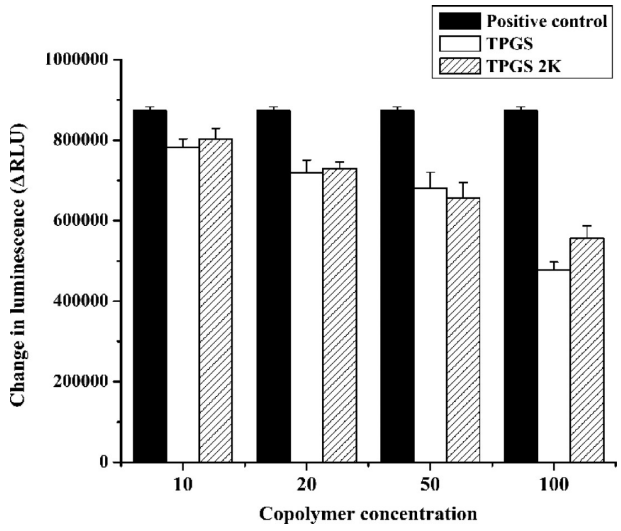

Figure 4. Inhibitory effect of TPGS 2K or TPGS on verapamil-stimulated P-gp ATPase activity. Verapamil (50 μM) was used alone as a positive control.

DOI: 10.1021/acsami.5b04995
ACS Appl. Mater. Interfaces 2015, 7, 18064−18075

Thus, inhibiting ATPase represents a universal intervention/regulation point for reversing MDR. TPGS and its analogues seem not to be a competitive inhibitor or a P-gp substrate as described in ref 36. So far, the widely accepted mechanisms of TPGS and its analogues actions are mainly based on the inhibition of P-gp after substrate-stimulated ATPase activation. TPGS and its analogues may limit the effectiveness of P-gp ATPase to hydrolyze ATP by blocking substrate binding, or binding to the ATPase-substrate complex, or P-gp allosteric modulation.[39,40] Put together, the ATPase assay data suggest that the inhibition of verapamil-stimulated ATPase activity induced by TPGS 2k plays a vital role in lowering the P-gp efflux liability. This inhibition can enhance the cellular uptake of the DOX-loaded TPGS 2K micelles to reverse P-gp-mediated MDR.

3.6. Determination of Mitochondrial Membrane Potential (MMP) and ATP Level. The effects of TPGS 2K or TPGS on the MMP and intracellular ATP level of MCF-7/ADR cells were investigated (Figure 5). The MMP was

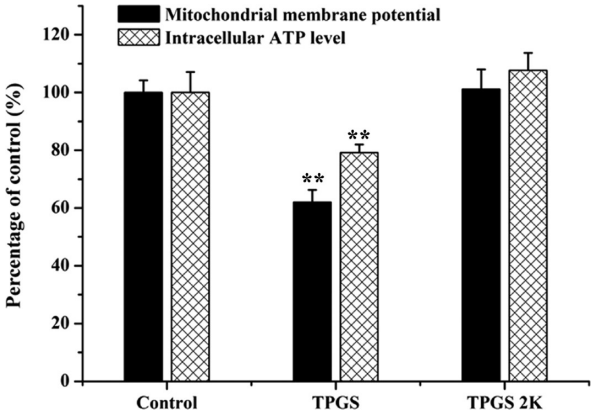

Figure 5. Effects of TPGS 2K or TPGS on the mitochondrial membrane potential and intracellular ATP level of MCF-7/ADR cells. Statistical significance: ** indicates $p < 0.01$.

determined by using a membrane permeable dye JC-1, which can selectively enter the mitochondria and change its fluorescent characters based on the aggregation form.[41] In present research, the mitochondrial depolarization (nonfunctional mitochondria) was monitored by measuring the decrease of the red/green fluorescence intensity ratio after incubation of MCF-7/ADR cells with TPGS or TPGS 2K (50 μM) for 3 h. The MCF-7/ADR cells treated with blank medium were used as the control. TPGS induced a significant decrease in the JC-1 red/green fluorescence intensity ratio to 62.06% compared with control group ($p < 0.01$), whereas no significant change in red/green fluorescence intensity ratio was observed for MCF-7/ADR cells treated with TPGS 2K ($p > 0.05$). The intracellular ATP level was then analyzed with luciferin/luciferase assay so as to further evaluate the influence of TPGS 2K or TPGS on the energy metabolism of MCF-7/ADR cells.[42] The MCF-7/ADR cells treated with blank medium were used as the control, and the ATP level was normalized as 100%. The TPGS resulted in a significant decrease in the intracellular ATP level to 79.15% of the control group ($p < 0.01$). In contrast, the ATP level (107.68%) of the MDR cells treated with the TPGS 2K was comparable to that of the control group ($P > 0.05$). These results on the intracellular ATP level assay were consistent with the mitochondrial membrane potential assay. The change in MMP was correlated with intracellular ATP depletion in MCF-7/ADR cells treated with TPGS or TPGS 2K. The MMP decrease and cellular ATP depletion induced by TPGS could be ascribed to the specific interaction of TPGS with mitochondrial organelles.[43] It was reported that VES and some VES analogs could interfere with the ubiquinone-binding sites of mitochondrial complex II in the respiratory chain. This effect destabilizes the mitochondrial membrane and thus destroys the energy supply of mitochondria.[28,44,45] However, in the present study, the TPGS 2K (at a concentration of 50 μM) did not induce significant changes on the MMP and intracellular ATP level. This may be due to the existence of longer PEG 2000 chain compared with TPGS. The difference of PEG chain length greatly influences the molecular physicochemical properties, such as size, molecular surface area, and polarity.[46,47] Such influence may be relevant to the effects of PEG-derivatized VES on modulating the MMP and intracellular ATP level in MCF-7/ADR cells. The definite mechanisms need further investigation.

3.7. Cytotoxicity Test. The cytotoxicity of free DOX solution, DOX-loaded TPGS 2K micelles, and corresponding blank micelles were assessed in MCF-7 and MCF-7/ADR cells using a MTT method (Figure 6). Blank TPGS 2K micelles showed certain cytotoxicity against MCF-7 and MCF-7/ADR cells (especially for MCF-7 cells) with the increase of polymeric concentration and incubation time. This result was consistent with that previously reported.[28] It may be ascribed to the unique apoptosis-inducing properties of VES or some VES analogs via the generation of reactive oxygen species (ROS) in tumor cells.[44,48,49] Free DOX solution showed significant cell cytotoxicity dependent on the drug concentration and the incubation time against MCF-7 cells. However, negligible cytotoxicity against MCF-7/ADR cells was observed for free DOX solution at 2.5−40 μg/mL after 24, 48, and 72 h incubation due to P-gp-mediated drug efflux.[25] In contrast, the cytotoxicity of the DOX-loaded TPGS 2K micelles was concentration- and incubation time-dependent in both MCF-7 and MCF-7/ADR cells. The DOX-loaded TPGS 2K micelles displayed higher therapeutic potency against MCF-7/ADR cells compared with free DOX solution.

IC50 values for all the DOX formulations were further calculated from the cytotoxicity data on MCF-7 and MCF-7/ADR cells (Table 2). The IC50 value of free DOX solution for MCF-7 cells was 2.92, 3.34, and 1.44-fold effective than that of DOX-loaded TPGS 2K micelles after 24, 48, 72 h treatment, respectively. It is seen that the free DOX solution showed advantages in achieving lower MCF-7 cell viability over the DOX-loaded TPGS 2K micelles. For MCF-7/ADR cells, the free DOX solution did not display apparent cytotoxicity at any of the designed drug concentrations and the incubation periods. In contrast, DOX-loaded TPGS 2K micelles induced significant cytotoxicity in MCF-7/ADR cells in a concentration-dependent tendency, and the IC50 values were 14.14, 8.78, and 5.77 μg/mL at 24, 48, and 72 h, respectively. Possible explanations for the above results are as follows. Polymeric micelles seem to provide a useful option for overcoming MDR by bypassing Pgp via endocytosis. This effect would aim in increasing the cellular DOX accumulation to exert stronger cytotoxic effect on MCF-7/ADR cells compared with free DOX solution. Furthermore, P-gp function inhibition also plays an important role in the cytotoxicity exhibited by DOX-loaded TPGS 2K micelles. TPGS 2K polymer can inhibit Verapamil-induced P-gp ATPase activity in a concentration-dependent manner, thereby further

DOI: 10.1021/acsami.5b04995
ACS Appl. Mater. Interfaces 2015, 7, 18064−18075

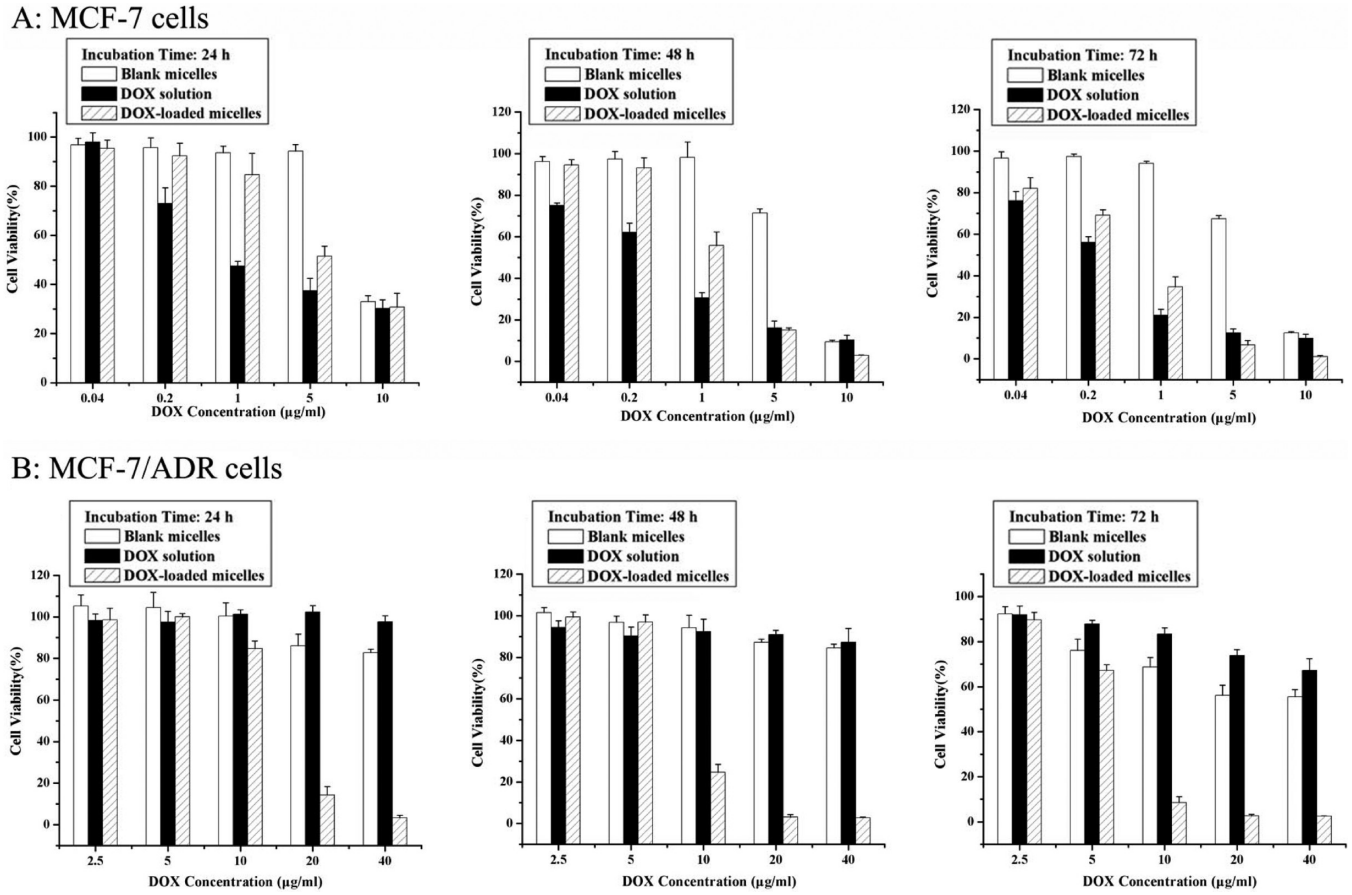

Figure 6. In vitro cytotoxicity of free DOX solution, DOX-loaded TPGS 2K micelles, and corresponding blank micelles against (A) MCF-7 and (B) MCF-7/ADR cancer cells after treatment for 24, 48, and 72 h.

Table 2. IC50 for Free DOX Solution and DOX-Loaded TPGS 2K Micelles to Inhibit Growth of MCF-7 and MCF-7/ADR Cells after 24, 48, and 72 h Incubation

time (h)	IC50 (μg/mL)			
	MCF-7 cells		MCF-7/ADR cells	
	DOX solution	TPGS 2K micelles	DOX solution	TPGS 2K micelles
24	1.69	4.93	N/A	14.14
48	0.32	1.07	N/A	8.78
72	0.25	0.36	N/A	5.77

promoting the cellular concentration of DOX to reverse P-gp-mediated MDR.

3.8. Cellular Uptake. Figure 7 shows the confocal laser scanning microscopy (CLSM) images of MCF-7 and MCF-7/ADR cells after 1 and 4 h treatment with DOX-loaded TPGS 2K micelles and free DOX solution at 10 μg/mL drug concentration. The cellular uptake of free DOX solution and DOX-loaded TPGS 2K micelles was time-dependent in MCF-7 cells (Figure 7A). After 1 h incubation, the DOX-loaded TPGS 2K micelles displayed stronger red fluorescence compared with free DOX solution. After 4 h incubation, the red fluorescence of free DOX solution was mainly distributed in nucleus. As for DOX-loaded TPGS 2K micelles, the red fluorescence was observed in both cytoplasm and nucleus. Both the unencapsulated DOX and the release of DOX from micelles during the incubation period contributed to the red fluorescence in the nucleus. Comparing with free DOX solution, MCF-7/ADR cells exposed to DOX-loaded TPGS 2K micelles exhibited much stronger red fluorescence in the cytoplasm around the nucleus in MCF-7/ADR cells after both 1 and 4 h incubation (Figure 7B). The results suggest that the encapsulation of DOX in micelles based on TPGS 2K conjugates could improve its accumulation in MCF-7/ADR cells and lead to an increase in therapeutic potency.

The cellular uptake of DOX-loaded TPGS 2K micelles (10 μg/mL drug concentration) by MCF-7 and MCF-7/ADR cells was further evaluated by flow cytometry and compared with free DOX solution (Figure 8). In MCF-7 cells, the DOX-loaded TPGS 2K micelles led to 1.72 and 1.11-fold higher cellular uptake compared with the free DOX solution after 1 and 4 h incubation, respectively (Figure 8A). As for MCF-7/ADR cells, the DOX encapsulation in TPGS 2K micelles led to 4.10- and 3.58-fold higher cellular uptake compared with the free DOX solution after 1 and 4 h incubation, respectively (Figure 8B). These results were consistent with the CLSM observation. It is reasonable that the endocytosis of DOX-loaded TPGS 2K micelles could result in a higher cellular uptake by bypassing P-gp-mediated efflux of MCF-7/ADR cells. Furthermore, as a nonionic surfactant derived from TPGS, TPGS 2K conjugates themselves have the ability to reverse MDR mediated by P-gp. It is helpful to further promote the DOX uptake in MCF-7/ADR cells. These results were consistent with the cytotoxicity assay.

3.9. In Vivo Imaging. The nude mice bearing MCF-7/ADR tumors were intravenously injected with the DiR-loaded

DOI: 10.1021/acsami.5b04995
ACS Appl. Mater. Interfaces 2015, 7, 18064−18075

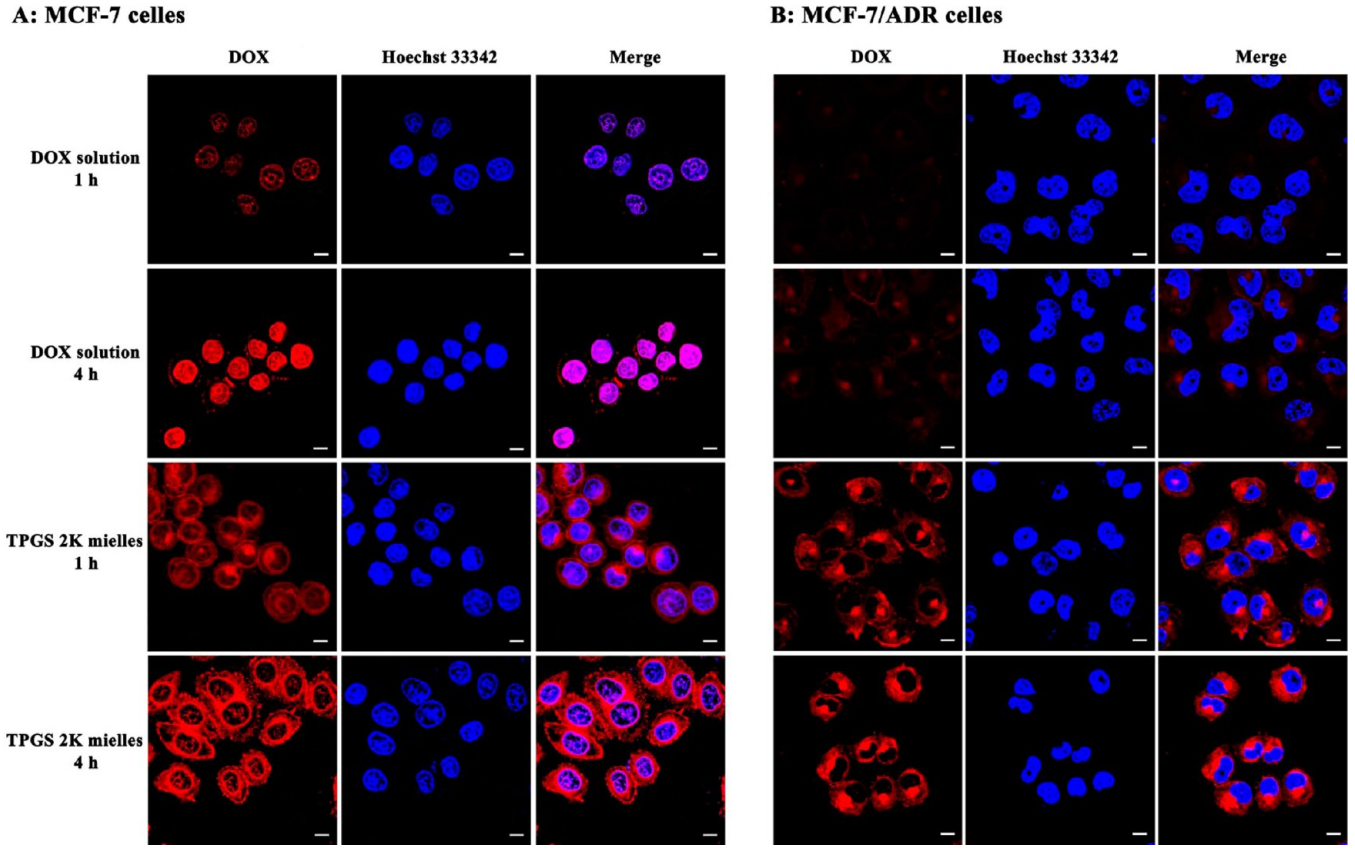

Figure 7. CLSM images of DOX-loaded TPGS 2K micelles and free DOX solution in (A) MCF-7 and (B) MCF-7/ADR cells after 1 and 4 h incubation. Blue and red colors indicate Hoechst 33342 and DOX, respectively (scale bar: 10 μm).

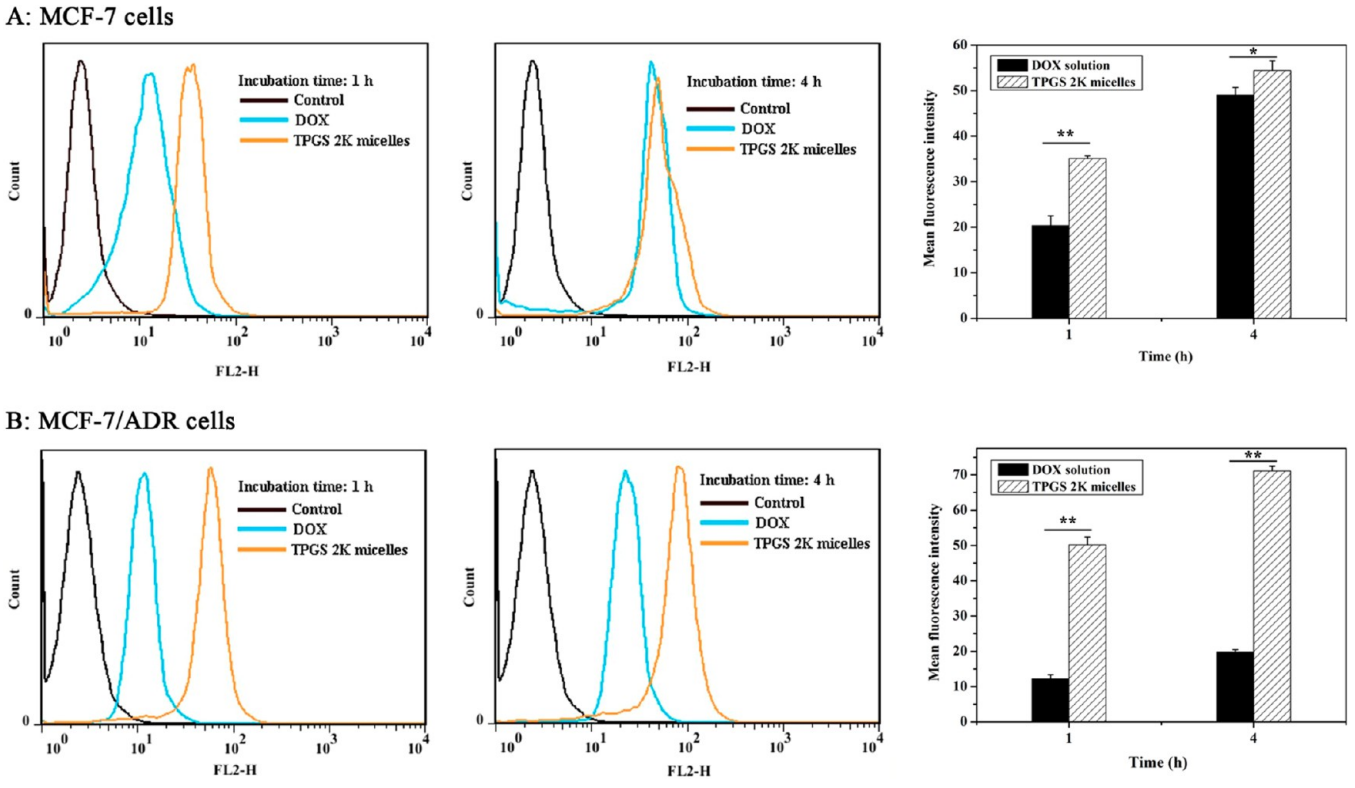

Figure 8. Flow cytometry measurement of the intracellular uptake of DOX in (A) MCF-7 and (B) MCF-7/ADR cells treated with DOX-loaded TPGS 2K micelles and free DOX solution. Statistical significance: * indicates $p < 0.05$; ** indicates $p < 0.01$.

DOI: 10.1021/acsami.5b04995
ACS Appl. Mater. Interfaces 2015, 7, 18064−18075

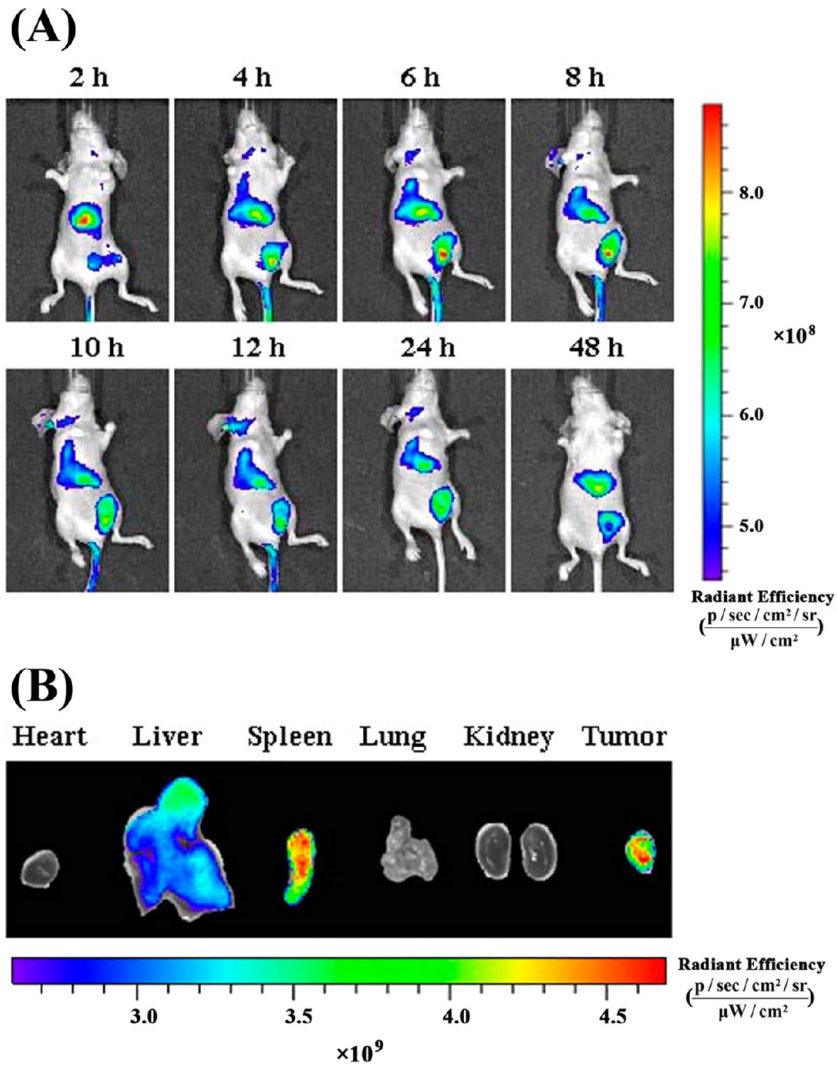

Figure 9. (A) In vivo imaging of MCF-7/ADR tumor-bearing nude mice injected with DiR-loaded TPGS 2K micelles at 2, 4, 6, 8, 10, 12, 24, and 48 h postinjection, respectively. (B) Ex vivo imaging of DiR-loaded TPGS 2K micelles in heart, liver, spleen, lung, kidney, and tumor of the nude mice bearing a MCF-7/ADR tumor at 48 h postinjection, respectively.

TPGS 2K micelles and observed using an optical image system. The live near-infrared fluorescent imaging of micelles in the live mice was monitored at 1, 2, 4, 8, 12, 24, and 48 h after intravenous injection (Figure 9). The DiR-loaded TPGS 2K micelles exhibited a significant fluorescence accumulation in the tumor site at 4 h after intravenous injection. The intense fluorescence signals were retained even 48 h following injection. The TPGS 2K micelles showed preferable distribution and slow elimination in the tumor region during the imaging period. The nanosize (<50 nm) of TPGS 2K micelles contributed for high fluorescence accumulation in the tumor site upon the EPR effect. The major organs (liver, heart, spleen, lung, and kidney) and tumor tissues were excised, and the ex vivo images (Figure 9) were further studied. No obvious fluorescence signals were observed in the heart, lung. and kidney tissues at 48 h after intravenous injection. The DiR-loaded TPGS 2K micelles were mainly accumulated in the tumor, liver, and spleen tissues. The relatively high fluorescent signals in spleen and liver may be due to the nonspecific capture by the reticuloendothelial system (RES).[50,51] In general, the TPGS 2K micelles demonstrated excellent passive targeting capacity to improve the accumulation of encapsulated cargo in the tumor region.

3.10. In Vivo Antitumor Effect. The in vivo antitumor efficacy of DOX-loaded TPGS 2K micelles and DOX solution was examined on nude mice bearing MCF-7/ADR tumor. At the experimental terminal after 13 days, the tumor volume was 84.87% (DOX solution group) and 40.80% (DOX-loaded micelles group) of control group, respectively (Figure 10B). Growth of tumor in nude mice treated with the DOX-loaded TPGS 2K micelles significantly slowed down compared with DOX solution group ($P < 0.01$) and saline group ($P < 0.01$). The DOX-loaded TPGS 2K micelles demonstrated better antitumor efficacy in inhibiting the tumor growth compared to the DOX solution. The tumor inhibition rate (TIR) was evaluated in terms of tumor weight (Figure 10C). The DOX solution and DOX-loaded TPGS 2K micelles exhibited tumor inhibiting capacity of 21.04% and 64.56% TIR, respectively. TPGS 2K micelles demonstrated better antitumor efficacy on MCF-7/ADR tumor xenografts compared with DOX solution. The in vivo antitumor results were consistent with the MDR reversal effects observed in the MTT assay and cellular uptake test. The body weight change was recorded simultaneously to

DOI: 10.1021/acsami.5b04995
ACS Appl. Mater. Interfaces 2015, 7, 18064−18075

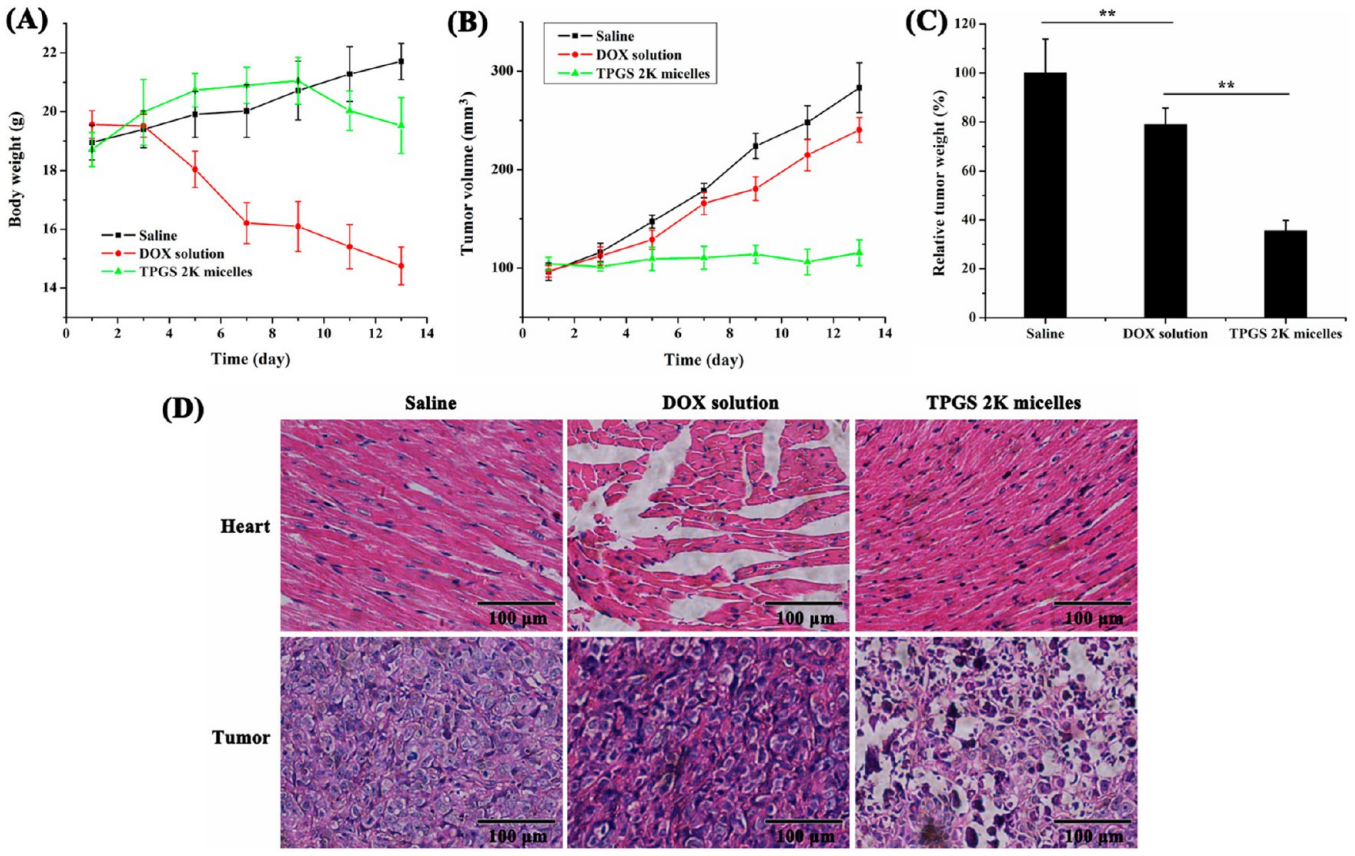

Figure 10. (A) Body weight changes of MCF-7/ADR tumor-bearing nude mice after intravenous injection of saline, DOX solution, and DOX-loaded TPGS 2K micelles. (B) Changes of tumor volume after treatment with saline, DOX solution, and DOX-loaded TPGS 2K micelles in tumor-bearing nude mice. (C) The weights of excised tumors from MCF-7/ADR tumor-bearing mice at the time of sacrifice. (D) Images of H&E-stained heart and tumor sections harvested from the mice after treatment with saline, DOX solution, and DOX-loaded TPGS 2K micelles. Statistical significance: ** indicates $p < 0.01$.

examine systemic toxicity (Figure 10A). Nude mice treated with DOX solution demonstrated 24.60% loss of initial weight with bad physical condition. In contrast, DOX-loaded TPGS 2K micelles caused a slight body weight loss compared to the saline group, indicating that DOX encapsulated in TPGS 2K micelles could decrease the systemic toxicity of DOX.

The heart and tumor issues were isolated from the tested mice and sectioned for pathology analysis (Figure 10D). DOX solution treated group exhibited severe cardiac tissue degeneration, necrosis of the muscle fibers, and cytoplasmic vacuolization. In contrast, there was no evidence of cardiotoxicity after DOX-loaded TPGS 2K micelles therapy compared to the saline group. The cardiotoxicity was significantly inhibited when DOX molecules were delivered by TPGS 2K micelles. To further evaluate the antitumor effect of DOX-loaded TPGS 2K micelles, the histopathology of the tumor from each group was also observed by H&E staining. In the saline group, the spherical or spindle-shaped tumor cells were polykaryocytes with large irregular nuclei and rich chromatin due to a rapid tumor growth. As for treatment groups, DOX-loaded TPGS 2K micelles resulted in more severe spotty necrosis with less cancer cells in the H&E stained tumor section compared to that under DOX solution treatment. This result revealed that the DOX-loaded TPGS 2K micelles were more effective than DOX solution in inhibiting the growth of MCF-7/ADR tumor xenografts in nude mice.

4. CONCLUSIONS

In summary, TPGS 2K conjugate, a TPGS analogue, was synthesized and applied as a micellar system formulating DOX for overcoming MDR. TPGS 2K conjugate exhibited an insignificant influence on the reduction of MMP and the depletion of intracellular ATP level of MCF-7/ADR cells but had evident effect on the inhibition of P-gp ATPase activity. The DOX-loaded TPGS 2K micelles demonstrated more efficient cellular uptake and higher cytotoxicity to inhibit the growth of MCF-7/ADR cells compared with DOX solution. In the in vivo distribution study using living imaging, the DiR-loaded TPGS 2K micelles exhibited excellent passive targeting capacity to improve the accumulation of encapsulated cargo in the tumor region. In the in vivo antitumor effect test, DOX-loaded TPGS 2K micelles significantly inhibited the growth of the MCF-7/ADR tumor and notably reduced the cardiotoxicity of DOX compared to DOX solution. Taken together, the amphiphilic TPGS 2k conjugate provides a promising polymeric material as a DOX-delivery vehicle to overcome MDR in cancer therapeutics.

■ ASSOCIATED CONTENT

Supporting Information

The authors declare that there are no conflicts of interest. The Supporting Information is available free of charge on the ACS Publications website at DOI: 10.1021/acsami.5b04995.

DOI: 10.1021/acsami.5b04995
ACS Appl. Mater. Interfaces 2015, 7, 18064−18075

FT-IR spectra of TPGS and TPGS 2K and plot of fluorescense intensity ratio from pyrene excitation spectra against the logarithmic concentration of TPGS 2K conjugate (PDF)

AUTHOR INFORMATION

Corresponding Author

*Address: College of Pharmacy, Dalian Medical University, 9 West Section, Lvshun South Road, Lvshunkou District, Dalian 116044, China. E-mail: lizhenpharm@126.com. Tel: +86-411-86110420. Fax: +86-411-86110420.

Notes

The authors declare no competing financial interest.

ACKNOWLEDGMENTS

This project was partly supported by the Natural Science Foundation of China (Grant 81302713).

REFERENCES

(1) Baguley, B. C. Multidrug Resistance in Cancer. *Methods Mol. Biol.* **2010**, *596*, 1−14.

(2) Gao, J.; Feng, S. S.; Guo, Y. Nanomedicine against Multidrug Resistance in Cancer Treatment. *Nanomedicine (London, U. K.)* **2012**, *7*, 465−468.

(3) Kathawala, R. J.; Gupta, P.; Ashby, C. R., Jr.; Chen, Z. S. The Modulation of ABC Transporter-mediated Multidrug Resistance in Cancer: a Review of the Past Decade. *Drug Resist. Updates* **2015**, *18*, 1−17.

(4) Binkhathlan, Z.; Lavasanifar, A. P-glycoprotein Inhibition as a Therapeutic Approach for Overcoming Multidrug Resistance in Cancer: Current Status and Future Perspectives. *Curr. Cancer Drug Targets* **2013**, *13*, 326−346.

(5) Liu, Y.; Fang, J.; Joo, K. I.; Wong, M. K.; Wang, P. Codelivery of Chemotherapeutics via Crosslinked Multilamellar Liposomal Vesicles to Overcome Multidrug Resistance in Tumor. *PLoS One* **2014**, *9*, e110611.

(6) Shaffer, B. C.; Gillet, J. P.; Patel, C.; Baer, M. R.; Bates, S. E.; Gottesman, M. M. Drug Resistance: Still a Daunting Challenge to the Successful Treatment of AML. *Drug Resist. Updates* **2012**, *15*, 62−69.

(7) Callaghan, R.; Luk, F.; Bebawy, M. Inhibition of the Multidrug Resistance P-glycoprotein: Time for a Change of Strategy? *Drug Metab. Dispos.* **2014**, *42*, 623−631.

(8) Torchilin, V. P. Structure and Design of Polymeric Surfactant-based Drug Delivery Systems. *J. Controlled Release* **2001**, *73*, 137−172.

(9) Maeda, H.; Bharate, G. Y.; Daruwalla, J. Polymeric Drugs for Efficient Tumor-targeted Drug Delivery Based on EPR-effect. *Eur. J. Pharm. Biopharm.* **2009**, *71*, 409−419.

(10) Xiao, H.; Song, H.; Yang, Q.; Cai, H.; Qi, R.; Yan, L.; Liu, S.; Zheng, Y.; Huang, Y.; Liu, T.; Jing, X. A Prodrug Strategy to Deliver Cisplatin(IV) and Paclitaxel in Nanomicelles to Improve Efficacy and Tolerance. *Biomaterials* **2012**, *33*, 6507−6519.

(11) Liu, Y.; Rohrs, J.; Wang, P. Advances and Challenges in the Use of Nanoparticles to Optimize PK/PD Interactions of Combined Anti-cancer Therapies. *Curr. Drug Metab.* **2014**, *15*, 818−828.

(12) Sakai-Kato, K.; Nishiyama, N.; Kozaki, M.; Nakanishi, T.; Matsuda, Y.; Hirano, M.; Hanada, H.; Hisada, S.; Onodera, H.; Harashima, H.; Matsumura, Y.; Kataoka, K.; Goda, Y.; Okuda, H.; Kawanishi, T. General Considerations Regarding the in Vitro and in Vivo Properties of Block Copolymer Micelle Products and Their Evaluation. *J. Controlled Release* **2015**, *210*, 76−83.

(13) Chavanpatil, M. D.; Patil, Y.; Panyam, J. Susceptibility of Nanoparticle- Encapsulated Paclitaxel to P-glycoprotein-mediated Drug Efflux. *Int. J. Pharm.* **2006**, *320*, 150−156.

(14) Kirtane, A. R.; Kalscheuer, S. M.; Panyam, J. Exploiting Nanotechnology to Overcome Tumor Drug Resistance: Challenges and Opportunities. *Adv. Drug Delivery Rev.* **2013**, *65*, 1731−1747.

(15) Batrakova, E. V.; Kabanov A. V. Pluronic Block Copolymers: Evolution of Drug Delivery Concept from Inert Nanocarriers to Biological Response Modifiers. *J. Controlled Release* **2008**, *130*, 98−106.10.1016/j.jconrel.2008.04.013

(16) Collnot, E. M.; Baldes, C.; Schaefer, U. F.; Edgar, K. J.; Wempe, M. F.; Lehr, C. M. Vitamin E TPGS P-glycoprotein Inhibition Mechanism: Influence on Conformational Flexibility, Intracellular ATP Levels, and Role of Time and Site of Access. *Mol. Pharmaceutics* **2010**, *7*, 642−651.

(17) Hong, W.; Chen, D.; Zhang, X.; Zeng, J.; Hu, H.; Zhao, X.; Qiao, M. Reversing Multidrug Resistance by Intracellular Delivery of Pluronic® P85 Unimers. *Biomaterials* **2013**, *34*, 9602−9614.

(18) Han, N.; Zhao, Q.; Wan, L.; Wang, Y.; Gao, Y.; Wang, P.; Wang, Z.; Zhang, J.; Jiang, T.; Wang, S. Hybrid Lipid-capped Mesoporous Silica for Stimuli-responsive Drug Release and Overcoming Multidrug Resistance. *ACS Appl. Mater. Interfaces* **2015**, *7*, 3342−3351.

(19) Zhang, Z.; Tan, S.; Feng, S. S. Vitamin E TPGS as a Molecular Biomaterial for Drug Delivery. *Biomaterials* **2012**, *33*, 4889−4906.

(20) Zhang, Z.; Feng, S. S. The Drug Encapsulation Efficiency, in Vitro Drug Release, Cellular Uptake and Cytotoxicity of Paclitaxel-loaded Poly(lactide)-tocopheryl Polyethylene Glycol Succinate Nanoparticles. *Biomaterials* **2006**, *27*, 4025−4033.

(21) Kulkarni, S. A.; Feng, S. S. Effects of Particle Size and Surface Modification on Cellular Uptake and Biodistribution of Polymeric Nanoparticles for Drug Delivery. *Pharm. Res.* **2013**, *30*, 2512−2522.

(22) Zhang, Z.; Lee, S. H.; Gan, C. W.; Feng, S. S. In Vitro and in Vivo Investigation on PLA-TPGS Nanoparticles for Controlled and Sustained Small Molecule Chemotherapy. *Pharm. Res.* **2008**, *25*, 1925−1935.

(23) Feng, S. S.; Mei, L.; Anitha, P.; Gan, C. W.; Zhou, W. Poly(lactide)-vitamin E Derivative/Montmorillonite Nanoparticle Formulations for the Oral Delivery of Docetaxel. *Biomaterials* **2009**, *30*, 3297−3306.

(24) Shieh, M. J.; Hsu, C. Y.; Huang, L. Y.; Chen, H. Y.; Huang, F. H.; Lai, P. S. Reversal of Doxorubicin-resistance by Multifunctional Nanoparticles in MCF-7/ADR cells. *J. Controlled Release* **2011**, *152*, 418−425.

(25) Li, Z.; Qiu, L.; Chen, Q.; Hao, T.; Qiao, M.; Zhao, H.; Zhang, J.; Hu, H.; Zhao, X.; Chen, D.; Mei, L. pH-sensitive Nanoparticles of Poly(L-histidine)-poly(lactide-co- glycolide)-tocopheryl Polyethylene Glycol Succinate for Anti-tumor Drug Delivery. *Acta Biomater.* **2015**, *11*, 137−150.

(26) Muthu, M. S.; Kulkarni, S. A.; Liu, Y.; Feng, S. S. Development of Docetaxel-loaded Vitamin E TPGS Micelles: Formulation Optimization, Effects on Brain Cancer Cells and Biodistribution in Rats. *Nanomedicine (London, U. K.)* **2012**, *7*, 353−364.

(27) Yu, L.; Bridgers, A.; Polli, J.; Vickers, A.; Long, S.; Roy, A.; Winnike, R.; Coffin, M. Vitamin E-TPGS Increases Absorption Flux of an HIV Protease Inhibitor by Enhancing its Solubility and Permeability. *Pharm. Res.* **1999**, *16*, 1812−1817.

(28) Mi, Y.; Liu, Y.; Feng, S. S. Formulation of Docetaxel by Folic Acid-conjugated d-α-tocopheryl Polyethylene Glycol Succinate 2000 (Vitamin E TPGS(2k)) Micelles for Targeted and Synergistic Chemotherapy. *Biomaterials* **2011**, *32*, 4058−4066.

(29) Hu, X.; Li, H.; Luo, S.; Liu, T.; Jiang, Y.; Liu, S. Thiol and pH Dual-responsive Dynamic Covalent Shell Cross-linked Micelles for Triggered Release of Chemotherapeutic Drugs. *Polym. Chem.* **2013**, *4*, 695−706.

(30) Cabral, H.; Matsumoto, Y.; Mizuno, K.; Chen, Q.; Murakami, M.; Kimura, M.; Terada, Y.; Kano, M. R.; Miyazono, K.; Uesaka, M.; Nishiyama, N.; Kataoka, K. Accumulation of Sub-100 nm Polymeric Micelles in Poorly Permeable Tumours Depends on Size. *Nat. Nanotechnol.* **2011**, *6*, 815−823.

(31) Cabral, H.; Kataoka, K. Progress of Drug-loaded Polymeric Micelles into Clinical Studies. *J. Controlled Release* **2014**, *190*, 465−476.

(32) Chen, Y.; Wu, Q.; Song, L.; He, T.; Li, Y.; Li, L.; Su, W.; Liu, L.; Qian, Z.; Gong, C. Polymeric Micelles Encapsulating Fisetin Improve

DOI: 10.1021/acsami.5b04995
ACS Appl. Mater. Interfaces 2015, 7, 18064−18075

the Therapeutic Effect in Colon Cancer. *ACS Appl. Mater. Interfaces* **2015**, *7*, 534−542.
(33) Wen, Y.; Meng, W. S. Recent In Vivo Evidences of Particle-Based Delivery of Small-Interfering RNA (siRNA) into Solid Tumors. *J. Pharm. Innov.* **2014**, *9*, 158−173.
(34) Wang, J.; Sun, J.; Chen, Q.; Gao, Y.; Li, L.; Li, H.; Leng, D.; Wang, Y.; Sun, Y.; Jing, Y.; Wang, S.; He, Z. Star-shape Copolymer of Lysine-linked Di-tocopherol Polyethylene Glycol 2000 Succinate for Doxorubicin Delivery with Reversal of Multidrug Resistance. *Biomaterials* **2012**, *33*, 6877−6888.
(35) Kataoka, K.; Matsumoto, T.; Yokoyama, M.; Okano, T.; Sakurai, Y.; Fukushima, S.; Okamoto, K.; Kwon, G. S. Doxorubicin-loaded Poly(ethylene glycol)-poly(beta- benzyl-L-aspartate) Copolymer Micelles: Their Pharmaceutical Characteristics and Biological Significance. *J. Controlled Release* **2000**, *64*, 143−153.
(36) Tang, J.; Fu, Q.; Wang, Y.; Racette, K.; Wang, D.; Liu, F. Vitamin E Reverses Multidrug Resistance in Vitro and in Vivo. *Cancer Lett.* **2013**, *336*, 149−157.
(37) Lu, J.; Huang, Y.; Zhao, W.; Chen, Y.; Li, J.; Gao, X.; Venkataramanan, R.; Li, S. Design and Characterization of PEG-derivatized Vitamin E as a Nanomicellar Formulation for Delivery of Paclitaxel. *Mol. Pharmaceutics* **2013**, *10*, 2880−2890.
(38) Prajapati, R.; Sangamwar, A. T. Translocation Mechanism of P-glycoprotein and Conformational Changes Occurring at Drug-binding Site: Insights from Multi-targeted Molecular Dynamics. *Biochim. Biophys. Acta, Biomembr.* **2014**, *1838*, 2882−2898.
(39) Wempe, M. F.; Wright, C.; Little, J. L.; Lightner, J. W.; Large, S. E.; Caflisch, G. B.; Buchanan, C. M.; Rice, P. J.; Wacher, V. J.; Ruble, K. M.; Edgar, K. J. Inhibiting Efflux with Novel Non-ionic Surfactants: Rational Design Based on Vitamin E TPGS. *Int. J. Pharm.* **2009**, *370*, 93−102.
(40) Lu, J.; Zhao, W.; Liu, H.; Marquez, R.; Huang, Y.; Zhang, Y.; Li, J.; Xie, W.; Venkataramanan, R.; Xu, L.; Li, S. An Improved D-α-tocopherol-based Nanocarrier for Targeted Delivery of Doxorubicin with Reversal of Multidrug Resistance. *J. Controlled Release* **2014**, *196*, 272−286.
(41) Sanpui, P.; Chattopadhyay, A.; Ghosh, S. S. Induction of Apoptosis in Cancer Cells at Low Silver Nanoparticle Concentrations using Chitosan Nanocarrier. *ACS Appl. Mater. Interfaces* **2011**, *3*, 218−228.
(42) Garewal, H. S.; Ahmann, F. R.; Schifman, R. B.; Celniker, A. ATP Assay: Ability to Distinguish Cytostatic from Cytocidal Anticancer Drug Effects. *J. Natl. Cancer Inst.* **1986**, *77*, 1039−1045.
(43) Yu, P.; Yu, H.; Guo, C.; Cui, Z.; Chen, X.; Yin, Q.; Zhang, P.; Yang, X.; Cui, H.; Li, Y. Reversal of Doxorubicin Resistance in Breast Cancer by Mitochondria-targeted pH-responsive Micelles. *Acta Biomater.* **2015**, *14*, 115−124.
(44) Neuzil, J.; Dong, L. F.; Ramanathapuram, L.; Hahn, T.; Chladova, M.; Wang, X. F.; Zobalova, R.; Prochazka, L.; Gold, M.; Freeman, R.; Turanek, J.; Akporiaye, E. T.; Dyason, J. C.; Ralph, S. J. Vitamin E Analogues as a Novel Group of Mitocans: Anti-cancer Agents that Act by Targeting Mitochondria. *Mol. Aspects Med.* **2007**, *28*, 607−645.
(45) Wang, D. F.; Rong, W. T.; Lu, Y.; Hou, J.; Qi, S. S.; Xiao, Q.; Zhang, J.; You, J.; Yu, S. Q.; Xu, Q. TPGS2k/PLGA Nanoparticles For Overcoming Multidrug Resistance by Interfering Mitochondria of Human Alveolar Adenocarcinoma Cells. *ACS Appl. Mater. Interfaces* **2015**, *7*, 3888−3901.
(46) Hugger, E. D.; Cole, C. J.; Raub, T. J.; Burton, P. S.; Borchardt, R. T. Automated Analysis of Polyethylene Glycol-induced Inhibition of P-glycoprotein Activity in Vitro. *J. Pharm. Sci.* **2003**, *92*, 21−26.
(47) Collnot, E. M.; Baldes, C.; Wempe, M. F.; Hyatt, J.; Navarro, L.; Edgar, K. J.; Schaefer, U. F.; Lehr, C. M. Influence of Vitamin E TPGS Poly(ethylene glycol) Chain Length on Apical Efflux Transporters in Caco-2 cell Monolayers. *J. Controlled Release* **2006**, *111*, 35−40.
(48) Ralph, S. J.; Rodríguez-Enríquez, S.; Neuzil, J.; Saavedra, E.; Moreno-Sánchez, R. The Causes of Cancer Revisited: "Mitochondrial Malignancy" and ROS-induced Oncogenic Transformation - Why Mitochondria are Targets for Cancer Therapy. *Mol. Aspects Med.* **2010**, *31*, 145−170.
(49) Wang, A. T.; Liang, D. S.; Liu, Y. J.; Qi, X. R. Roles of Ligand and TPGS of Micelles in Regulating Internalization, Penetration and Accumulation against Sensitive or Resistant Tumor and Therapy for Multidrug Resistant Tumors. *Biomaterials* **2015**, *53*, 160−172.
(50) Balducci, A.; Wen, Y.; Zhang, Y.; Helfer, B. M.; Hitchens, T. K.; Meng, W. S.; Wesa, A. K.; Janjic, J. M. A Novel Probe for the Non-invasive Detection of Tumor-associated Inflammation. *Oncoimmunology.* **2013**, *2*, e23034.
(51) Qin, C.; He, B.; Dai, W.; Lin, Z.; Zhang, H.; Wang, X.; Wang, J.; Zhang, X.; Wang, G.; Yin, L.; Zhang, Q. The Impact of a Chlorotoxin-modified Liposome System on Receptor MMP-2 and the Receptor-associated Protein ClC-3. *Biomaterials* **2014**, *35*, 5908−5920.

DOI: 10.1021/acsami.5b04995
ACS Appl. Mater. Interfaces 2015, 7, 18064−18075